



Orthogonal long-period fiber grating for directly exciting the orbital angular momentum

ZHAO LIU,^{1,2} GUOXUAN ZHU,^{1,2} YALI LI,^{1,2} JIAN YU,^{1,2} ZHIYONG BAI,^{1,2,*} SHEN LIU,^{1,2} JUN HE,^{1,2} AND YIPING WANG^{1,2}

¹Shenzhen Key Laboratory of Photonic Devices and Sensing Systems for Internet of Things, College of Physics and Optoelectronic Engineering, Shenzhen University, Shenzhen 518060, China

²Guangdong and Hong Kong Joint Research Centre for Optical Fibre Sensors, Shenzhen University, Shenzhen 518060, China

*baizhiyong@szu.edu.cn

Abstract: An orthogonal long-period fiber grating (OLPFG) is proposed and demonstrated for directly exciting the orbital angular momentum (OAM), without the need for other devices. This grating was produced using CO₂ laser exposure in the orthogonal direction. A helical phase was then optically induced in the OLPFG, with a chirality determined by the structure of the OLPFG. In this study, ± 1 -order OAM resonances were respectively observed in OLPFGs with a different orthogonal direction. The conversion efficiency of OAM mode in this process was 99%, and the purity was higher than 98%. In addition, incident light in any polarization state was observed to excite OAM with the same polarization.

© 2020 Optical Society of America under the terms of the [OSA Open Access Publishing Agreement](#)

1. Introduction

Optical beams with a helical phase carry orbital angular momentum (OAM) with unique properties that have been widely studied in a diverse range of fields [1–3]. The helical phase front can be described as $\exp(il\varphi)$, where φ is the azimuthal angle and l is the topological charge [4]. This helical structure exhibits a phase singularity at the center of the beam, exhibiting unique characteristics that have been applied in optical tweezers [5], nanoscale microscopy [6], optical trapping [7], and fiber communications [8–10].

There are currently several different techniques (and devices) used to generate OAM-carrying beams, including spiral phase plates [11], cylindrical lens mode converters [1,12], q-plates [13–14], and spatial light modulators (SLMs) [15]. The most common approach uses an SLM for helical phase front modulation. However, the use of SLMs is limited by physical size and alignment difficulties. As such, a compact and convenient device capable of OAM mode generation would be highly beneficial. Fiber grating-based OAM converters have attracted increased attention recently, due to their high stability, small size, and compatibility with fiber communication systems. Three types of fiber grating-based OAM converters have been reported to date, including acousto-optic modulation gratings [16–19], conventional long-period fiber gratings (LPGs) with assistant devices [20–26], and helical fiber gratings (HFGs) [27–30]. Acousto-optic modulation gratings have demonstrated good flexibility for wavelength tuning. However, low stability and external equipment requirements limit their practical application. Conventional LPGs excite $\pm l$ OAM simultaneously, thereby requiring additional equipment to extract the desired mode. In contrast, HFGs can directly excite OAM without any other devices, offering robust applicability. However, fabricating HFGs is a complex process that requires perfectly melting the fiber and includes highly sensitive mechanical twisting. As such, only a few research groups have successfully reported high quality HFGs.

In this study, an OLPFG is proposed for direct excitation of OAM in light without the use of auxiliary equipment. This OLPFG was achieved using a CO₂ laser separately incident on two sides of a fiber in the orthogonal direction. The resulting intensity patterns and phase

fronts of the coupled modes were experimentally investigated. Results showed that the proposed OLPGs successfully induced an annular intensity distribution and a helical phase in beams. The chirality of the OAM beams was determined by the spatial order of the orthogonal exposure. The polarization characteristics and purity of the OAM beams were also tested. Results showed that the produced polarization was consistent with that of the incident beam, with a measured purity higher than 98% for any incident polarization state.

2. Experimental procedures and phenomena

The fabrication process for the OLPG was divided into two steps. First, one side of the fiber was exposed to CO₂ laser using two-dimension scanning technology. After this unilateral exposure, the grating coupling intensity was increased to >3 dB and the translation stage automatically returned to the initial location. The processed fiber was then rotated by 90° using a pair of fiber rotators. The first step was repeated on the orthogonal side of the fiber. Key fabrication parameters were as follows. A 17 g weight was suspended from one end of the fiber to maintain constant stress along the fiber axis during the etching process. The resulting OLPG pitch was $\Lambda=970$ μm and the number of grating periods was $N=30$. The experimental samples were commercial two-mode step index fibers (YOCC), the CO₂ laser energy was 340 mW. Figure 1 shows a schematic diagram of the proposed OLPG, in which the yellow arrow indicates the direction of laser irradiation, and the black arrow represents the inscribed direction, that is, the z-axis direction. Figure 1(a) shows the exposure on one side of the fiber after the first step, represented by the red pattern. Figure 1(b) shows the fabricated OLPG after the second orthogonal exposure step, indicated by the yellow pattern. The fiber rotation direction in the second step can be clockwise (CW) or counterclockwise (CCW). Figure 1(c) illustrates two types of exposure combinations that produced clockwise and counterclockwise OLPGs, denoted as C-OLPGs and CC-OLPGs, respectively. The helical phase of OAM beams was measured after excitation from OLPGs with a CW and CCW exposure orientation. The corresponding interference patterns produced between the coupled OAM modes and the co-axis Gaussian beams are shown in Fig. 1(d). These CW and CCW interference patterns indicate that -1- and +1-order OAM modes were successfully produced by the C-OLPG and CC-OLPG, respectively.

In the experiment, the OLPG transmission spectrum was monitored using an optical spectrum analyzer (OSA) assisted by a broadband spontaneous emission light source. Figures 2(a) and 2(b) show the transmission spectra for the C-OLPG and CC-OLPG, with peak excitation resonance wavelengths of 1576.2 nm and 1575.4 nm and depths of 30.67 dB and 28.27 dB, respectively. The OLPG coupling efficiency was higher than 99% and the insertion loss was less than 1 dB. There is an evident difference in the resonance wavelengths of the C-OLPG and CC-OLPG, which may have resulted from power instability in the CO₂ laser. Figure 2 also shows the mode field patterns at the resonant peak (a_1 , b_1) and at the midsection (a_2 , a_3 , b_2 , b_3), which exhibit an apparent ring-like profile.

The helical phase and OAM mode polarization characteristics were investigated using the configuration shown in Fig. 3. Incident light from a tunable laser was divided into two beams by a polarization beam splitter (PBS). One of the beams, after passing through a polarizer and a series of wave plates, was incident on the OLPG and used to excite the OAM modes. The other beam was used as a reference signal. The two beams then combined and interfered at a beam splitter, followed by a CCD. The first polarizer (P1) and quarter-wave plate (QWP1) were jointly used to generate a circular polarization state in the input light. It is noted that, the QWP1 will be replaced by a Half-wave plates (HWP1) when the effect of linearly polarized light on OAM generation was investigated in experiment. HWP1 and HWP2 were used to adjust the polarization direction of linearly polarized light. A quarter-wave plate (QWP2) and a polarizer (P2) were used to analyze polarization characteristics for light output from the OLPG sample.

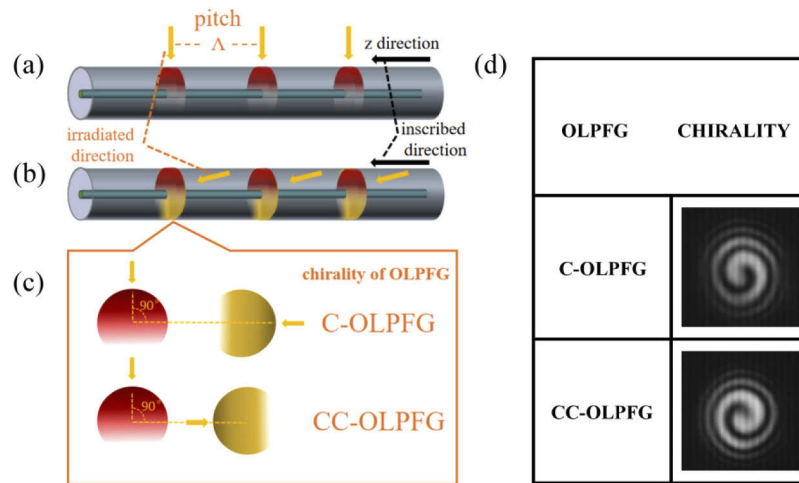


Fig. 1. Schematic diagram of formation principle of OLPG. The yellow arrow indicates the laser irradiation direction, and the black arrow indicates the LPFG inscribing direction. Structure diagram of the (a) the first exposure and (b) the second orthogonal exposure; (c) Schematic diagram of exposure combination of C-OLPG and CC-OLPG; (d) interference patterns between the coupled OAM modes in two types of OLPGs and co-axis Gaussian beams.

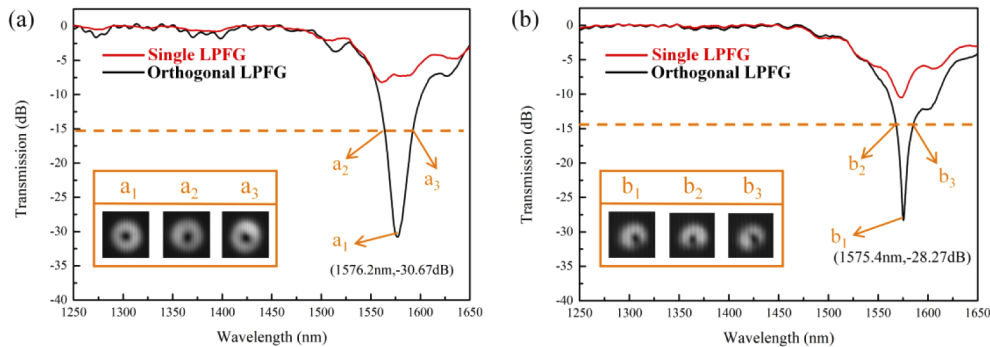


Fig. 2. Transmission spectra of (a) C-OLPG and (b) CC-OLPG, the red curve represents the spectrum of a single LPFG, and the black curve represents the spectrum of an orthogonal LPFG, and mode field patterns at the resonant peak (a_1, b_1) and at the midsection (a_2, a_3, b_2, b_3).

Polarizer 3 (P3) filtered the reference light to produce a linear polarization state. The resulting intensity distribution and interference pattern were then measured with a CCD.

The system described above was used to investigate the helical phase and polarization characteristics of OAM modes excited by the proposed OLPGs. The transparent axis direction of P1 is parallel to the polarization direction of the PBS output beam. The measured intensity distribution in the coupled OAM modes and the interference pattern between the two beams are shown in Fig. 4. The incident light was linearly polarized and focused directly into the OLPG. In-LP^{||} and In-LP[⊥] in Fig. 4(a) respectively denote two orthogonal polarization directions for the input light, which were adjusted using HWP1. Out-LP^{||} and Out-LP[⊥] respectively indicate the orthogonal polarization states of the resulting OAM modes, detected by P2. It is worth noting that the polarization directions denoted by In-LP^{||} and Out-LP^{||} were consistent with

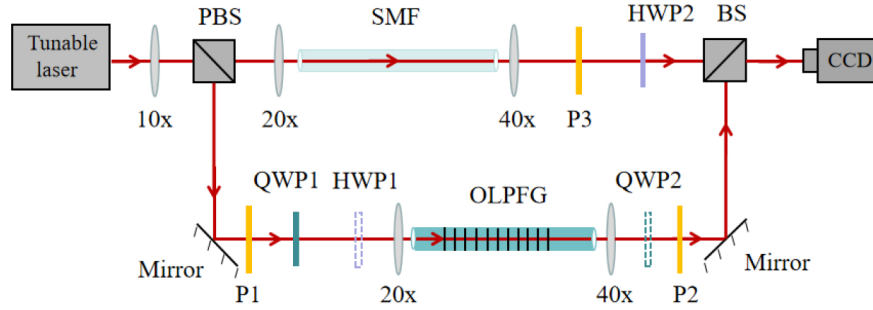


Fig. 3. Schematic diagram of the experimental setup used for detecting OAM modes in OLPGs. PBS, polarized beam splitter; BS, beam splitter; QWP1, quarter-wave plate 1; QWP2, quarter-wave plate 2; HWP1, half-wave plate 1; HWP2, half-wave plate 2; P1, polarizer 1; P2, polarizer 2 and P3, polarizer 3.

that of P1. As a result, mode profiles and interference patterns were clearly observed when the transparent axis direction of P2 was the same as that of the incident light. In other words, OLPGs excite the input Gaussian beam with a linear polarization to an OAM beams with the

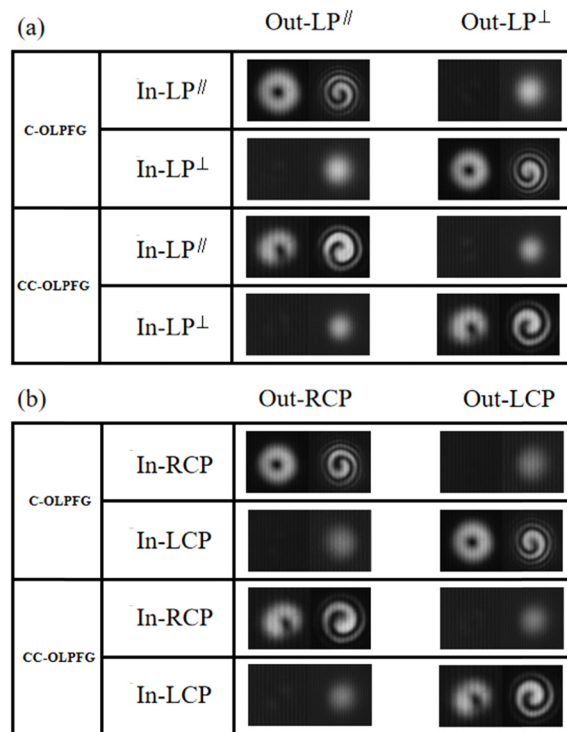


Fig. 4. Mode field distribution and interference pattern distribution for the ± 1 -order OAM modes generated by the C-OLPG at a resonant wavelength of 1576.2nm and by the CC-OLPG at a resonant wavelength of 1575.4nm while input (a) linearly polarized light and (b) circularly polarized light. The leftmost column shows the devices with different chirality, and the second column on the left shows the input light with different polarization states. The top line represents the polarization state of the OAM beam.

same polarization state. Left- and right-handed circularly polarized (LCP/RCP) input light was produced by adjusting the angle between the transparent axis of P1 and the fast axis of QWP1. The intensity distribution of the resulting OAM and corresponding interference patterns are shown in Fig. 4(b). In-RCP/In-LCP and Out-RCP/Out-LCP represent the circular polarization states of the input light and the coupled OAM, respectively. These results were collected by P2 and acquired by converting the polarization of output OAM modes to linear polarization states with QWP2. The measured results in Fig. 4(b) show that the circular OAM modes were obtained, and their polarization states matching that of the input light as well.

The spiral interference pattern observed between ± 1 -order OAM modes and the reference beams, indicates the relationship between grating structure and chirality of helical phase. Figure 4 shows the clockwise pattern formed in C-OLPFG, indicating a -1-order OAM beam was excited. The counterclockwise pattern in CC-OLPFG indicates the presence of +1-order OAM beams. Output beams from the OLPFG were also measured using other incident polarization states, producing the same results. This suggests the OLPFGs directly excite OAM modes in arbitrary input light polarization states, the chirality of which is determined by the grating structure. The resulting polarization states are the same as that of the input light, which could allow OAM beams to be flexibly applied in areas such as micro-operations and optical communications.

The system shown in Fig. 5 was used to measure the purity of the resulting OAM modes. The OAM beam was incident on an SLM, which was loaded with fork grating holograms of varying orders to generate $l = -2, -1, 0, +1$, and $+2$ helical phases, the inset in Fig. 5 shows a 1st-order fork grating. A polarizer (P1) and a quarter-wave plate (QWP) were used to regulate the polarization state of the input light. A half-wave plate (HWP) was used to change the polarization direction of the OAM beam, ensuring it was parallel to the polarization response of the SLM. The purity of OAM modes excited by the OLPFG was measured using linearly polarized, LCP, and RCP light. The results for C-OLPFG and CC-OLPFG are shown in Figs. 6(a1) and 6(a2), respectively. We tested the contribution of each component to the OAM mode by recording the energy intensity in the center of the conversion light. The power ratio was also calculated to determine the purity of each mode. As seen in Figs. 6(b1) and 6(b2), the purity of both C-OLPFG and CC-OLPFG was higher than 98% for every incident light polarization.

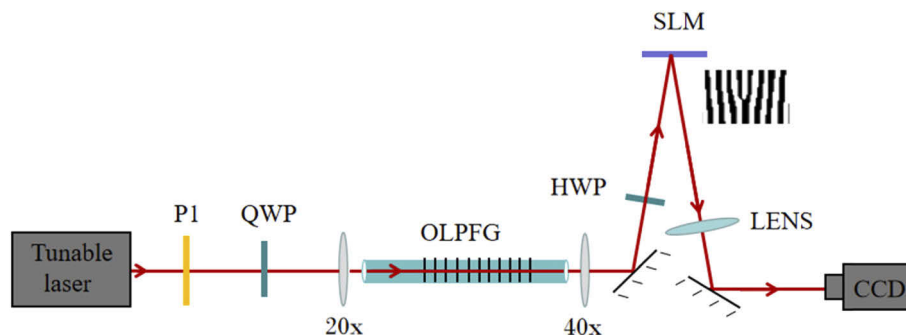


Fig. 5. Experimental system for measuring the purity of OAM mode excited by OLPFG. P1, polarizer 1; QWP, quarter-wave plate; HWP, half-wave plate; SLM, spatial light modulator.

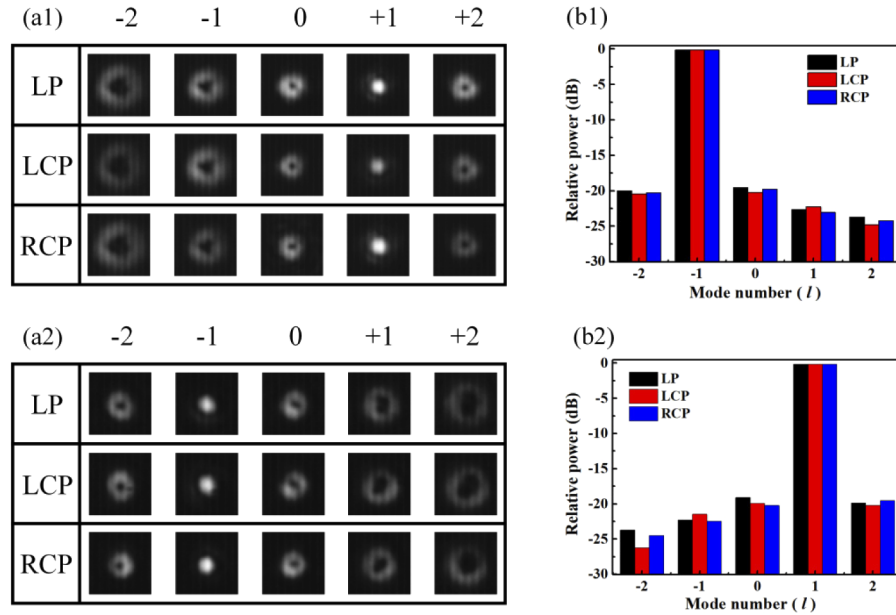


Fig. 6. Mode profiles occurring as a series of helical phase with $l = -2, -1, 0, +1$ and $+2$, added to the generated OAM modes for the (a1) C-OLPFG and (a2) CC-OLPFG for LP, RCP and LCP into light polarization states. Also shown are the power ratios for each component in the OAM modes generated in the (b1) C-OLPFG and (b2) CC-OLPFG.

3. Discussion

The OAM excitation in orthogonal grating can be explained as follows. Generally, in an LPFG-based ± 1 -order OAM generator, OAM modes result from the coherent superposition of 1st-order even and odd modes with a phase delay of $\pi/2$ [16–26]. Thereinto, the orthogonal modes and the phase delay between them are realized by twisting and lateral squeezing the fiber, respectively. In this work, the OLPG can be considered as two independent LPFGs, and thus, the two superposition modes can be directly coupled by these two orthogonal LPFGs [19], respectively. The phase delay may result from the slight dislocation between the two LPFGs [31–32], which is originated in the tension of fiber stretched by a suspended weight during the fabricating process.

During the fabrication of the OLPG, the coupling strength of the first LPFG is more than 3dB, and thus, the power of the fundamental mode was partly coupled into the 1st-order core mode, and then the remained fundamental mode and 1st-order core mode propagated together in the fiber. When the second LPFG is inscribed, the remained fundamental mode was coupled into the 1st-order mode with an orthogonal polarization state. At this time, the resonance peak coupling depth is greater than 25dB, indicating that the coupling efficiency of the grating is high. The phase difference $\Delta\varphi$ between the two orthogonal 1st-order modes can be expressed as Eq. (1):

$$\Delta\varphi = (\beta_{01} - \beta_{11}) \times \Delta z \quad (1)$$

where Δz is the dislocation between two gratings, β_{01} and β_{11} are the propagation constants of fundamental mode and 1st-order mode, respectively. When the phase difference $\Delta\varphi$ meets Eq. (2), the OAM mode with a topological charge number of ± 1 can be obtained by superimposing the orthogonal modes.

$$\Delta\varphi = (2q + 1) \times \frac{\pi}{2} \quad (2)$$

where q is an integer and can be positive or negative. When q takes 0 or other positive values, we calibrate that the second LPFG has a dislocation in the $+z$ direction ($\Delta z > 0$) relative to the first LPFG. When q takes a negative value, there is a dislocation in the $-z$ direction ($\Delta z > 0$). Thus, according to Eqs. (1) and (2), the value of $\Delta\varphi$, that is, the chirality of OAM is dependent on the size or sign of Δz . In experiment, the tension of the fiber is constant during the OLPGF fabrication, that is, the size of Δz is constant, and thus, the chirality of the OAM can be designed by changing the rotation direction of the fiber in the second preparation step. Moreover, Eqs. (1) and (2) indicated that, an ideal value of Δz is expected to generate a phase delay of $\pi/2$. However, due to the combined effect of large radiation area of CO₂ laser and large error tolerance of LPFG in pitch, even if there has deviation in the angle and Δz between the two gratings, a higher purity OAM mode can be still obtained in experiment.

4. Conclusion

An OAM mode generator based on an OLPGF has been proposed and experimentally demonstrated. Gaussian beams were directly converted to OAM beams of order $l = \pm 1$ with a high conversion efficiency (99%). The measured polarization characteristics of the OAM beam were consistent with that of the input light, achieving the purity higher than 98%. These results suggest the proposed OLPGF is a simple, low-cost OAM mode generator that can directly produce $l = \pm 1$ order OAM beams, even higher-order OAM modes. As such, the device could be widely used in optical fiber communication and particle control.

Funding

National Natural Science Foundation of China (61635007, 61875134); Natural Science Foundation of Guangdong Province (2017A030310033, 2018KQNCX219); Science, Technology and Innovation Commission of Shenzhen Municipality (JCYJ20170412105604705, JCYJ20180507182058432); Shenzhen University (grant no. 2019097).

Disclosures

The authors declare that there are no conflicts of interest related to this article.

References

1. L. Allen, M. W. Beijersbergen, R. J. C. Spreeuw, and J. P. Woerdman, "Orbital angular momentum of light and transformation of Laguerre Gaussian Laser modes," *Phys. Rev. A* **45**(11), 8185–8189 (1992).
2. M. R. Dennis, K. O'Holleran, and M. J. Padgett, "Chapter 5 Singular Optics: Optical Vortices and Polarization Singularities," *Prog. Opt.* **53**, 293–363 (2009).
3. S. Ramachandran and P. Kristensen, "Optical vortices in fiber," *Nanophotonics* **2**(5-6), 455–474 (2013).
4. A. M. Yao and M. J. Padgett, "Orbital angular momentum: Origins, behavior and applications," *Adv. Opt. Photonics* **3**(2), 161–204 (2011).
5. D. G. Grier and Y. Han, "Erratum: Vortex rings in a constant electric field," *Nature* **424**(6946), 267–268 (2003).
6. S. Fühapter, A. Jesacher, S. Bernet, and M. Ritsch-Marte, "Spiral interferometry," *Opt. Lett.* **30**(15), 1953–1955 (2005).
7. M. Chen, M. Mazilu, Y. Arita, E. M. Wright, and K. Dholakia, "Dynamics of microparticles trapped in a perfect vortex beam," *Opt. Lett.* **38**(22), 4919–4922 (2013).
8. S. Ramachandran, P. Gregg, P. Kristensen, and S. E. Golowich, "On the scalability of ring fiber designs for OAM multiplexing," *Opt. Express* **23**(3), 3721–3730 (2015).
9. A. E. Willner, H. Huang, Y. Yan, Y. Ren, N. Ahmed, G. Xie, C. Bao, L. Li, Y. Cao, Z. Zhao, J. Wang, M. P. J. Lavery, M. Tur, S. Ramachandran, A. F. Molisch, N. Ashrafi, and S. Ashrafi, "Optical communications using orbital angular momentum beams," *Adv. Opt. Photonics* **7**(1), 66–106 (2015).
10. S. Li and J. Wang, "A Compact Trench-Assisted Multi-Orbital-Angular-Momentum Multi-Ring Fiber for Ultrahigh-Density Space-Division Multiplexing (19 Rings \times 22 Modes)," *Sci. Rep.* **4**(1), 3853 (2015).
11. M. W. Beijersbergen, R. P. C. Coerwinkel, M. Kristensen, and J. P. Woerdman, "Helical-wavefront laser beams produced with a spiral phaseplate," *Opt. Commun.* **112**(5-6), 321–327 (1994).
12. J. Courtial and M. J. Padgett, "Performance of a cylindrical lens mode converter for producing Laguerre-Gaussian laser modes," *Opt. Commun.* **159**(1-3), 13–18 (1999).

13. D. Naidoo, F. S. Roux, A. Dudley, I. Litvin, B. Piccirillo, L. Marrucci, and A. Forbes, "Controlled generation of higher-order Poincaré sphere beams from a laser," *Nat. Photonics* **10**(5), 327–332 (2016).
14. L. Marrucci, C. Manzo, and D. Paparo, "Optical spin-to-orbital angular momentum conversion in inhomogeneous anisotropic media," *Phys. Rev. Lett.* **96**(16), 163905 (2006).
15. N. R. Heckenberg, R. McDuff, C. P. Smith, and A. G. White, "Generation of optical phase singularities by computer-generated holograms," *Opt. Lett.* **17**(3), 221–223 (1992).
16. K. Wei, W. Zhang, L. Huang, D. Mao, F. Gao, T. Mei, and J. Zhao, "Generation of cylindrical vector beams and optical vortex by two acoustically induced fiber gratings with orthogonal vibration directions," *Opt. Express* **25**(3), 2733–2741 (2017).
17. W. Zhang, L. Huang, K. Wei, P. Li, B. Jiang, D. Mao, F. Gao, T. Mei, G. Zhang, and J. Zhao, "High-order optical vortex generation in a few-mode fiber via cascaded acoustically driven vector mode conversion," *Opt. Lett.* **41**(21), 5082–5085 (2016).
18. W. Zhang, K. Wei, L. Huang, D. Mao, B. Jiang, F. Gao, G. Zhang, T. Mei, and J. Zhao, "Optical vortex generation with wavelength tunability based on an acoustically-induced fiber grating," *Opt. Express* **24**(17), 19278–19285 (2016).
19. P. Z. Dashti, F. Alhassen, and H. P. Lee, "Observation of Orbital Angular Momentum Transfer between Acoustic and Optical Vortices in Optical Fiber," *Phys. Rev. Lett.* **96**(4), 043604 (2006).
20. H. Wu, S. Gao, B. Huang, Y. Feng, X. Huang, W. Liu, and Z. Li, "All-fiber second-order optical vortex generation based on strong modulated long-period grating in a four-mode fiber," *Opt. Lett.* **42**(24), 5210–5213 (2017).
21. S. Liu, Y. Zhang, C. Fu, Z. Bai, Z. Li, C. Liao, Y. Wang, J. He, Y. Liu, and Y. Wang, "Temperature Insensitivity Polarization-Controlled Orbital Angular Momentum Mode Converter Based on an LPFG Induced in Four-Mode Fiber," *Sensors* **18**(6), 1766–1774 (2018).
22. S. Li, Q. Mo, X. Hu, C. Du, and J. Wang, "Controllable all-fiber orbital angular momentum mode converter," *Opt. Lett.* **40**(18), 4376–4379 (2015).
23. Y. Han, Y. Liu, Z. Wang, W. Huang, L. Chen, H. Zhang, and K. Yang, "Controllable all-fiber generation/conversion of circularly polarized orbital angular momentum beams using long period fiber gratings," *Nanophotonics* **7**(1), 287–293 (2018).
24. Y. Zhao, T. Wang, C. Mou, Z. Yan, Y. Liu, and T. Wang, "All-fiber Vortex Laser Generated With Few-Mode Long-Period Gratings," *IEEE Photonics Technol. Lett.* **30**(8), 752–755 (2018).
25. Y. Jiang, G. Ren, Y. Lian, B. Zhu, W. Jin, and S. Jian, "Tunable orbital angular momentum generation in optical fibers," *Opt. Lett.* **41**(15), 3535–3538 (2016).
26. Y. Zhao, Y. Liu, L. Zhang, C. Zhang, J. Wen, and T. Wang, "Mode converter based on the long-period fiber gratings written in the two-mode fiber," *Opt. Express* **24**(6), 6186–6195 (2016).
27. C. Fu, S. Liu, Z. Bai, J. He, C. Liao, Y. Wang, Z. Li, Y. Zhang, K. Yang, B. Yu, and Y. Wang, "Orbital Angular Momentum Mode Converter Based on Helical Long Period Fiber Grating Inscribed by Hydrogen-Oxygen Flame," *J. Lightwave Technol.* **36**(9), 1683–1688 (2018).
28. H. Zhao, P. Wang, T. Yamakawa, and H. Li, "All-fiber second-order orbital angular momentum generator based on a single-helix helical fiber grating," *Opt. Lett.* **44**(21), 5370–5373 (2019).
29. C. Fu, S. Liu, Y. Wang, Z. Bai, J. He, C. Liao, Y. Zhang, F. Zhang, B. Yu, S. Gao, Z. Li, and Y. Wang, "High-Order orbital angular momentum mode generator based on twisted photonic crystal fiber," *Opt. Lett.* **43**(8), 1786–1789 (2018).
30. Y. Zhang, Z. Bai, C. Fu, S. Liu, J. Tang, J. Yu, C. Liao, Y. Wang, J. He, and Y. Wang, "Polarization-independent orbital angular momentum generator based on a chiral fiber grating," *Opt. Lett.* **44**(1), 61–64 (2019).
31. X. Zhang, A. Wang, R. Chen, H. Ming, and W. Zhao, "Generation of optical vortices by a pair of optical fiber orthogonal-dislocated gratings," *J. Opt.* **21**(8), 085707 (2019).
32. X. Zhang, A. Wang, R. Chen, Y. Zhou, H. Ming, and Q. Zhan, "Generation and conversion of higher order optical vortices in optical fiber with helical fiber Bragg gratings," *J. Lightwave Technol.* **34**(10), 2413–2418 (2016).